The Astrophysical Journal Letters, 750:L9 (6pp), 2012 May 1 doi:10.1086/2041-8205/750/1/L9

HARMONIC IN-PAINTING OF COSMIC MICROWAVE BACKGROUND SKY BY CONSTRAINED GAUSSIAN REALIZATION

Jaiseung Kim[1], Pavel Naselsky[1], and Nazzareno Mandolesi[2]
[1] Niels Bohr Institute & Discovery Center, Blegdamsvej 17, DK-2100 Copenhagen, Denmark; jkim@nbi.dk
[2] INAF/IASF, Istituto di Astrofisica Spaziale e Fisica Cosmica di Bologna, Istituto Nazionale di Astrofisica, via Gobetti 101, I-40129 Bologna, Italy
Received 2012 February 1; accepted 2012 March 26; published 2012 April 11

ABSTRACT

The presence of astrophysical emissions between the last scattering surface and our vantage point requires us to apply a foreground mask on cosmic microwave background (CMB) sky maps, leading to large cuts around the Galactic equator and numerous holes. Since many CMB analysis, in particular on the largest angular scales, may be performed on a whole-sky map in a more straightforward and reliable manner, it is of utmost importance to develop an efficient method to fill in the masked pixels in a way compliant with the expected statistical properties and the unmasked pixels. In this Letter, we consider the Monte Carlo simulation of a constrained Gaussian field and derive it CMB anisotropy in harmonic space, where a feasible implementation is possible with good approximation. We applied our method to simulated data, which shows that our method produces a plausible whole-sky map, given the unmasked pixels, and a theoretical expectation. Subsequently, we applied our method to the *Wilkinson Microwave Anisotropy Probe* foreground-reduced maps and investigated the anomalous alignment between quadrupole and octupole components. From our investigation, we find that the alignment in the foreground-reduced maps is even higher than the Internal Linear Combination map. We also find that the *V*-band map has higher alignment than other bands, despite the expectation that the *V*-band map has less foreground contamination than other bands. Therefore, we find it hard to attribute the alignment to residual foregrounds. Our method will be complementary to other efforts on in-painting or reconstructing the masked CMB data, and of great use to *Planck* surveyor and future missions.

Key words: cosmic background radiation – methods: data analysis – methods: statistical

Online-only material: color figures

1. INTRODUCTION

Several astrophysical emission sources exist between the last scattering surface and our vantage point. Due to contamination from the "foregrounds," we need to apply proper masking on microwave sky maps, which leads to cuts of varying widths around the Galactic equator and numerous holes. Since many cosmic microwave background (CMB) analysis, in particular on the largest angular scales, may be performed on a whole-sky map in a more straightforward and reliable manner, there have been several efforts to reconstruct a whole-sky map from incomplete sky data (Efstathiou 2004; Bielewicz et al. 2004; de Oliveira-Costa & Tegmark 2006; Feeney et al. 2011). However, the fidelity of reconstruction is limited, because it is not possible to reliably reconstruct harmonics modes mainly confined to the Galactic cuts (Bielewicz et al. 2004). Therefore, there have been active attempts to fill in the missing information in CMB sky data with a priori (Abrial et al. 2008; Inoue et al. 2008; Bucher & Louis 2011).

Historically, the act of recovering damaged parts of valuable paintings by a skilled restoration artist is called "in-painting." In digital imaging, there are various in-painting methods (Masnou 2002; Ballester et al. 2001; Bertalmo et al. 2003; Rane et al. 2003). While these methods work well for images of periodic or predictable patterns, they may not be suitable for CMB data, which have random Gaussian nature. On the other hand, there have been works on generating constrained Gaussian fields, which have been used in the study of large-scale structures (Bertschinger 1987; Hoffman & Ribak 1992, 1991). However, it is not feasible for the pixel data of the *Wilkinson Microwave Anisotropy Probe* (*WMAP*) or *Planck* surveyor, which amounts to millions of pixels or more. In this Letter, we are going to implement the method for CMB anisotropy in harmonic space, where the computational load may be significantly reduced with good approximation. After demonstrating it with simulated data, we are going to apply our method to the *WMAP* foreground-reduced maps and investigate the well-known anomaly associated with the quadrupole and octupole component. Throughout this Letter, we will use the term "in-painting" to denote our described procedure.

The outline of this Letter is as follows. In Section 2, we briefly discuss CMB anisotropy in harmonic space and the effect of incomplete sky coverage. In Section 3, we discuss the simulation of a constrained Gaussian field and its implementation in CMB anisotropy in harmonic space. In Section 4, we apply our method to simulated data and present the result. In Section 5, we apply our method to masked *WMAP* data and investigate the multipole vector alignment between the quadrupole and octupole. In Section 6, we summarize our work.

2. CMB ANISOTROPY IN HARMONIC SPACE

CMB anisotropy over the whole sky is conveniently decomposed in terms of spherical harmonics:

$$T(\hat{\mathbf{n}}) = \sum_{lm} a_{lm}\, Y_{lm}(\hat{\mathbf{n}}), \tag{1}$$

where a_{lm} and $Y_{lm}(\theta, \phi)$ are a decomposition coefficient and a spherical harmonic function, respectively, and $\hat{\mathbf{n}}$ denotes a sky direction. In most inflationary models, decomposition coefficients of CMB anisotropy follow the Gaussian distribution

of the following statistical properties:

$$\langle a_{lm} \rangle = 0, \tag{2}$$

$$\langle a_{lm} a^*_{l'm'} \rangle = \delta_{ll'} \delta_{mm'} C_l, \tag{3}$$

where $\langle \ldots \rangle$ denotes the average over an ensemble of universes, and C_l denotes CMB power spectrum. Accordingly, the CMB anisotropies $T(\theta, \phi)$, which follows Gaussian distribution, have the following angular correlation:

$$\langle T(\hat{\mathbf{n}})\ T(\hat{\mathbf{n}}') \rangle = \sum_l \frac{2l+1}{4\pi} W_l\, C_l\, P_l(\cos\theta), \tag{4}$$

where P_l is a Legendre polynomials and $\theta = \cos^{-1}(\hat{\mathbf{n}} \cdot \hat{\mathbf{n}}')$.

In the presence of a foreground mask, the spherical coefficients of a masked sky $\tilde{a}_{lm}$ are related to those of a whole sky as follows:

$$\tilde{a}_{l_3 m_3} = \sum_{l_2 m_2} F(l_2, m_2, l_3, m_3)\, a_{l_2 m_2}, \tag{5}$$

where

$$F(l_2, m_2, l_3, m_3) = (-1)^{m_3} \sqrt{\frac{2l_3+1}{4\pi}} \sum_{l_1 m_1} \sqrt{(2l_1+1)(2l_2+1)} \times \begin{pmatrix} l_1 & l_2 & l_3 \\ m_1 & m_2 & -m_3 \end{pmatrix} \times \begin{pmatrix} l_1 & l_2 & l_3 \\ 0 & 0 & 0 \end{pmatrix} w_{l_1 m_1}, \tag{6}$$

$$w_{l_1 m_1} = \int Y^*_{l_1 m_1}(\theta, \phi)\, W(\theta, \phi)\, d\Omega, \tag{7}$$

and $W(\theta, \phi)$ is the mask function, which is zero inside the mask and one elsewhere, and the terms within the big parentheses being Wigner 3j symbols. Using Equations (3) and (5), we may easily show the following correlation between a_{lm} and $\tilde{a}_{l'm'}$:

$$\langle a_{lm}\, \tilde{a}^*_{l'm'} \rangle = F^*(l, m, l', m')\, C_l, \tag{8}$$

$$\langle \tilde{a}_{l'm'}\, \tilde{a}^*_{l''m''} \rangle = \sum_{lm} F^*(l, m, l', m')\, F(l, m, l,'' m'')\, C_l. \tag{9}$$

3. IN-PAINTING IN HARMONIC SPACE

Hoffman & Ribak (1991) developed an efficient algorithm to simulate constrained Gaussian fields. According to their work, we may simulate a Gaussian random field $f(\mathbf{r})$ under constraints $f(\mathbf{r}_j)$ with the following:

$$f(\mathbf{r}) = f_{\rm mc}(\mathbf{r}) + \sum_{ij} \mathbf{b}_i\ (\mathbf{C}^{-1})_{ij}\, (f(\mathbf{r}_j) - f_{\rm mc}(\mathbf{r}_j)), \tag{10}$$

where

$$\mathbf{b}_i = \langle f(\mathbf{r})\, f(\mathbf{r}_i) \rangle,$$
$$\mathbf{C}_{ij} = \langle f(\mathbf{r}_i)\, f(\mathbf{r}_j) \rangle,$$

and the subscript "mc" denotes an unconstrained Gaussian Monte Carlo simulation. Applying Equation (10) to CMB pixel data, we may fill in the masked pixel data with plausible values. The procedure has been extensively studied and discussed by (Bucher & Louis 2011). Though in a slightly different context, the power spectrum estimation by Gibbs sampling, which includes generating an underlying CMB map according to the conditional distribution, has some overlapping (Wandelt et al. 2004; Eriksen et al. 2004).

As seen in Equation (4), pixel correlation exists at a wide range of separation angles, which makes us take into account a tremendous amount of pixels even just to fill in a single pixel. Therefore, we may not readily apply the method to the *WMAP* or *Planck* data, which have millions of pixels. Noting the CMB anisotropies in harmonic space (i.e., a_{lm}) are expected to follow Gaussian distribution, we may consider implementing the constrained Gaussian realization in harmonic space. In this case, we draw each a_{lm} from the constraints, which are masked spherical harmonic coefficients $\tilde{a}_{l'm'}$. Rewriting Equation (10) explicitly for spherical harmonic coefficients yields:

$$a_{lm} = a^{\rm mc}_{lm} + \mathbf{b}\, \mathbf{C}^{-1}\, (\tilde{\boldsymbol{a}} - \tilde{\boldsymbol{a}}^{\rm mc}), \tag{11}$$

where $\tilde{\boldsymbol{a}}$ is a column vector consisting of $\tilde{a}_{l'm'}$ and

$$\mathbf{b} = \langle a_{lm}\, \tilde{\boldsymbol{a}}^\dagger \rangle,$$
$$\mathbf{C} = \langle \tilde{\boldsymbol{a}}\, \tilde{\boldsymbol{a}}^\dagger \rangle,$$

and $\tilde{a}_{lm}$ is a spherical harmonic coefficient of the masked sky (cf. Equation (5)) and $\dagger$ denotes a complex conjugate transpose. Given Equations (8) and (9), this process by Equation (11) may seem computationally prohibitive. However, for a widely used foreground mask such as KQ85, the magnitudes of $w_{l_1 m_1}$ are significant only at the lowest multipoles (i.e., $|w_{l_1 \gg 1, m_1}| \approx 0$). For such a mask, we may easily show $F^*(l, m, l', m') \approx 0$ for $|l - l'| \gg 1$, using $|w_{l_1 \gg 1, m_1}| \approx 0$ and the triangular inequalities of Wigner 3j symbol $|l_3 - l_2| \leqslant l_1$ (cf. Equation (8)). It is worth the noting that $F^*(l, m, l', m')$ approaches $\delta_{ll'} \delta_{mm'}$ in the limit of a complete sky coverage (i.e., $w_{l_1 > 0, m_1} = 0$). Using this result with Equation (8), we may subsequently show $\langle a_{lm}\, \tilde{a}^*_{l'm'} \rangle$ for $|l - l'| \gg 1$. In other words, a_{lm} are nearly independent of $\tilde{a}_{l'm'}$, if the multipole numbers l and l' differ significantly. Therefore, for a constrained simulation of a_{lm} by Equation (11), we need to consider only constraints $\tilde{a}_{l'm'}$ of multipoles not far away from a_{lm}. With this finding, we may significantly reduce the computational cost involved with Equation (11), and effectively in-paint a masked CMB sky map. We may summarize the procedure as follows: first, we generate unconstrained $a^{\rm mc}_{lm}$ by Monte Carlo simulation, and then transform them by Equation (11). From the result of Equation (11), we synthesize a CMB anisotropy map $T(\theta, \phi)$, as necessary. Throughout this Letter, we will refer to this procedure as "in-painting."

4. APPLICATION TO SIMULATED DATA

In order to test our method, we generated simulated CMB data, where we assumed the *WMAP* concordance ΛCDM model and the *WMAP* beam smoothing at *V* band (Komatsu et al. 2011; Jarosik et al. 2011). We set the simulation to contain multipoles up to 700, and produced it with the HEALPix pixellization $N_{\rm side} = 512$ (Gorski et al. 1999; Gorski et al. 2005). We masked the simulated data by the *WMAP* KQ85, which admits pixel data of sky fractions 78%. At the top of Figure 1, we show the simulated map with the foreground mask applied. We applied the procedure described in the previous section to the masked simulated data, and generated a whole-sky map.

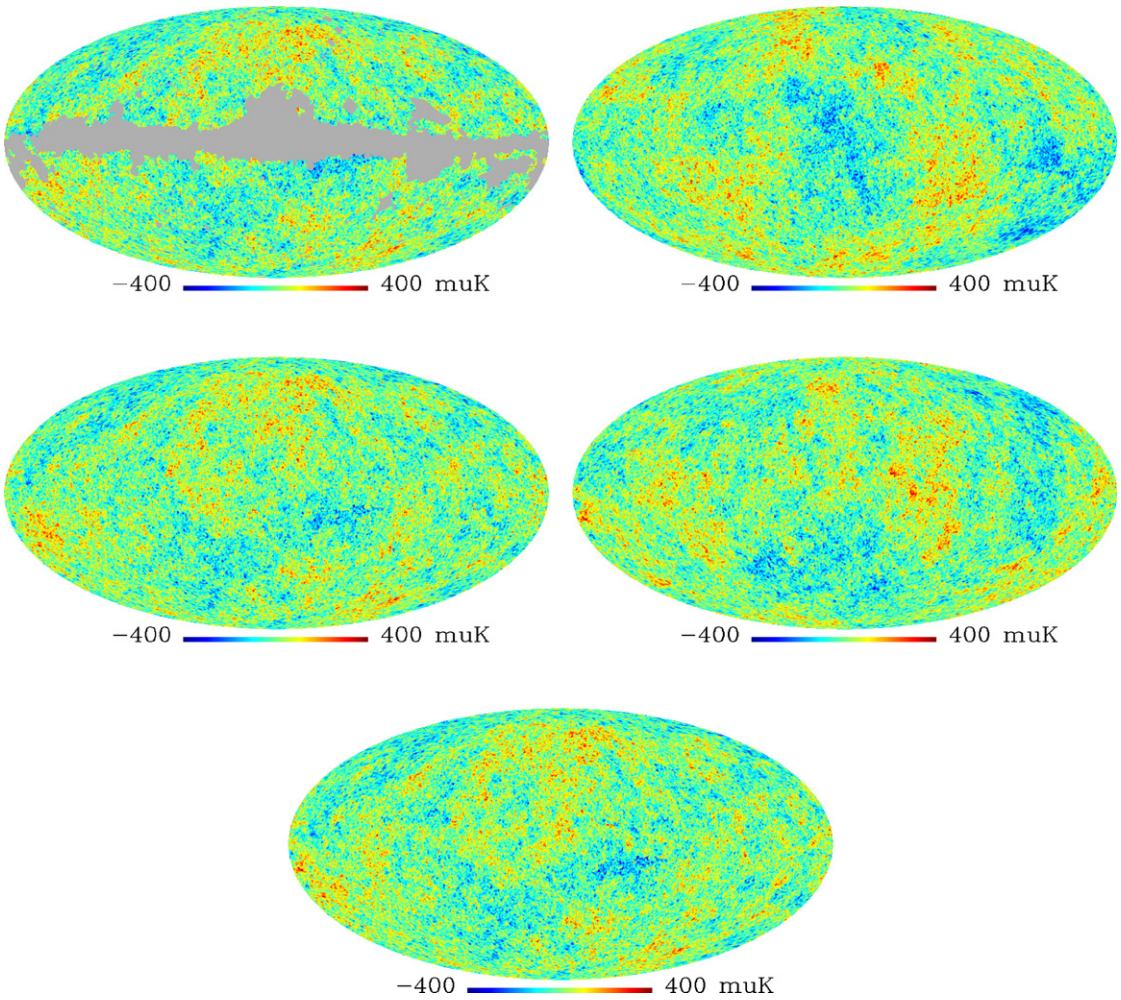

Figure 1. Simulated input map with the KQ85 mask applied (top), unconstrained realization and constrained realization (the second and the third), another set of an unconstrained realization and a constrained realization (the fourth and bottom): the constrained realizations are obtained by the Equation (11) with the preceding unconstrained realization, respectively.

(A color version of this figure is available in the online journal.)

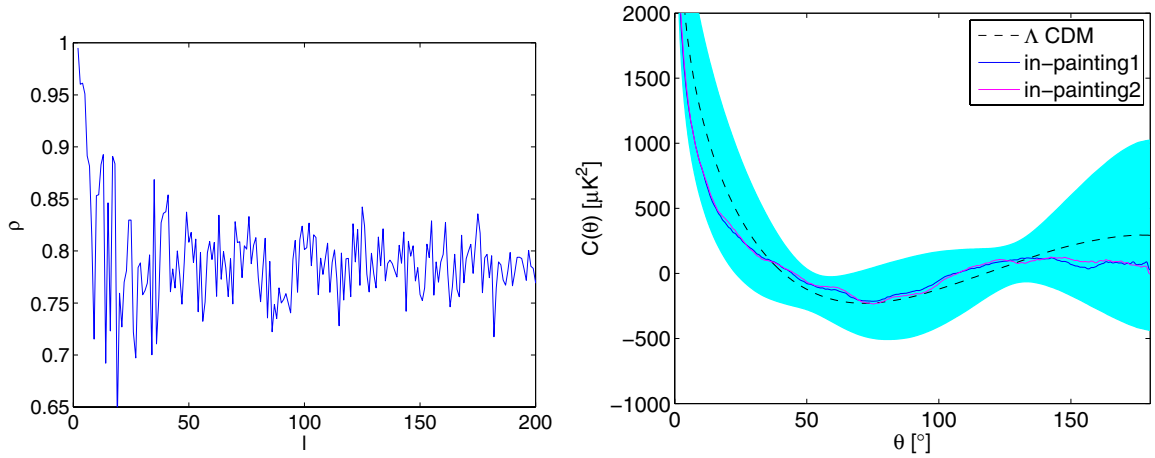

Figure 2. Cross-correlation between in-painted maps for each multipole (top) and angular autocorrelation of in-painted maps (bottom).

(A color version of this figure is available in the online journal.)

In Figure 1, we show two constrained realizations obtained by Equation (11), where we used different unconstrained realizations for the "mc" terms in Equation (11). We like to stress that both of the results are equally likely, given the constraints. In Figure 2, we show the correlation between two in-painted maps, which is computed for each multipole as follows:

$$\rho = \frac{\sum_m \mathrm{Re}[a_{1,lm}\,(a_{2,lm})^*]}{\sqrt{\sum_{m'} |a_{1,lm'}|^2 \sum_{m''} |a_{2,lm''}|^2}}, \quad (12)$$

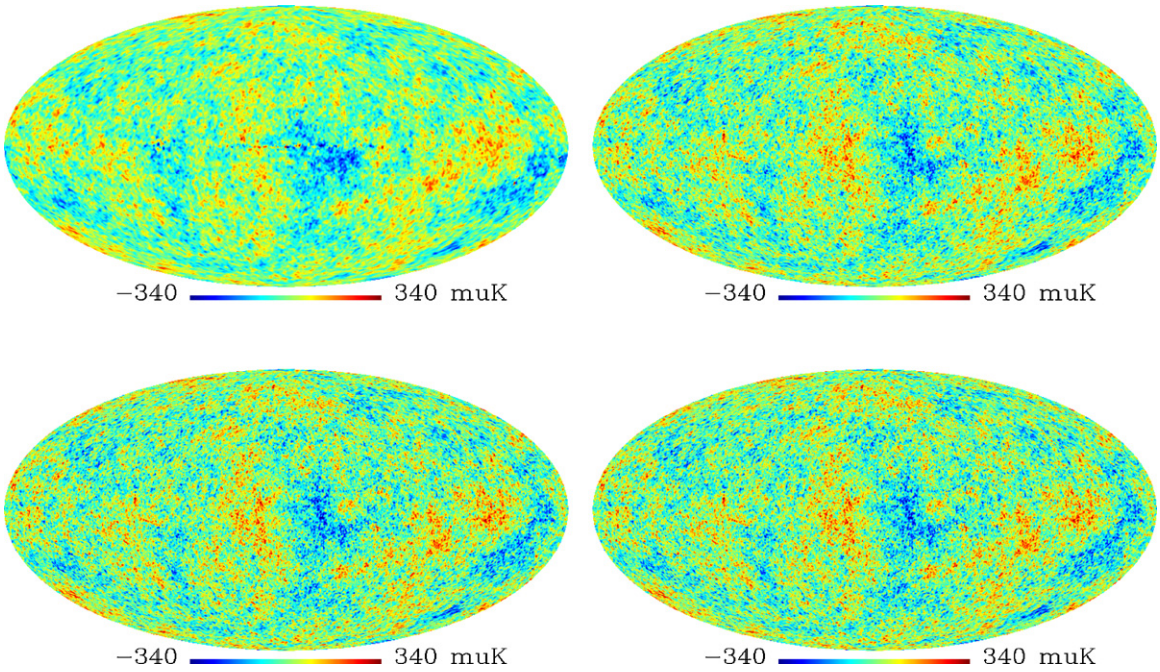

Figure 3. ILC map (top) and in-painted maps of the Q, V, and W bands (from the second to the last).
(A color version of this figure is available in the online journal.)

where "1" and "2" in the subscripts denote two results, respectively. As shown in Figure 2, we see there is strong convergence at low multipoles, which also stays strong at higher multipoles. If we used a less conservative foreground mask, which, for instance, is constituted of large holes around the Galactic plane like a Swiss cheese, the level of convergence will be even stronger. Nonetheless, given the random Gaussian nature of CMB anisotropy, it is not possible to reconstruct the exact realization, which happens to be our universe. Therefore, our intention is filling-in the missing information in a way compliant with the expected statistical properties. However, we do not presumably expect the statistical properties of in-painted maps to be very close to the theoretical prediction, due to the statistical fluctuation associated with cosmic variance.

In order to see whether our in-painted maps, indeed, are consistent with the expected statistical properties, we estimated the angular correlations, which are plotted in Figure 2. In the same plot, we show the angular correlation of the *WMAP* concordance model (Komatsu et al. 2011), where the dotted line and shaded region denote the theoretical prediction and 2σ ranges, as determined by Monte Carlo simulations. As shown in Figure 2, we find that the angular correlation of our in-painted maps are well inside the shaded region. We also find that the angular correlation of in-painted maps are similar to each other, which agrees with the strong convergence previously shown.

5. APPLICATION TO THE *WMAP* DATA

In order to reduce foregrounds, the *WMAP* team subtracted diffuse foregrounds by template fitting, and produced "foreground-reduced maps," which are available at the Q, V, and W bands, respectively (Gold et al. 2011). Besides the foreground-reduced maps, there is the Internal Linear Combination (ILC) map, which is usually used without foreground masking. In spite of contamination from bright point sources and Galactic foregrounds, the difficulty of investigating the lowest multipoles on masked sky data made the whole-sky ILC widely used for the investigation of CMB data anomalies (de Oliveira-Costa et al. 2004; Copi et al. 2004, 2006, 2010, 2011; Schwarz et al. 2004; Land & Magueijo 2005a, 2005b, 2007; Rakić & Schwarz 2007; Coles et al. 2004; Chiang et al. 2003; Kim & Naselsky 2010a, 2010b; Hansen et al. 2011; Naselsky et al. 2011, 2012). However, foreground-reduced maps with a foreground mask is more reliable and contains less foreground contamination than the ILC map. Therefore, it is worth investigating the anomaly at the lowest multipoles, using the foreground-reduced maps.

Using our method, we in-painted the masked foreground-reduced maps. The in-painting process is the same as the one described in the previous sections, except that C_l in Equation (9) should be replaced by $C_l + N_l$, with N_l being the power spectrum of instrument noise. We simulated instrument noise with the *WMAP* noise model $\sigma_0/\sqrt{N_{\rm obs}}$ (Jarosik et al. 2011), and estimated the noise power spectrum N_l from 1000 simulated noise maps, where $N_{\rm obs}$ is the number of observations for a pixel and σ_0 is 2197, 3137, and 6549 [μK] for the Q, V, and W bands, respectively. For the foreground mask, we used the *WMAP* team's KQ85 mask.

In Figure 3, we show the whole-sky ILC map and our in-painted maps. Note that in-painted maps have the beam smoothing of the original maps, which are distinct at each band. In particular, the beam smoothing of the ILC map, which corresponds to FWHM $= 1^\circ$, differs most significantly from the others. From the in-painted maps, we estimated the quadrupole and octupole components, which are shown in Figure 4. For comparison, we show the quadrupole and octupole components of the *WMAP* ILC map. It is interesting to note that the amplitudes of the quadrupole and the octupole anisotropies are greater and smaller than the ILC map, respectively, which will alleviate the anomaly of low quadrupole power and the parity asymmetry (de Oliveira-Costa et al. 2004; Kim & Naselsky

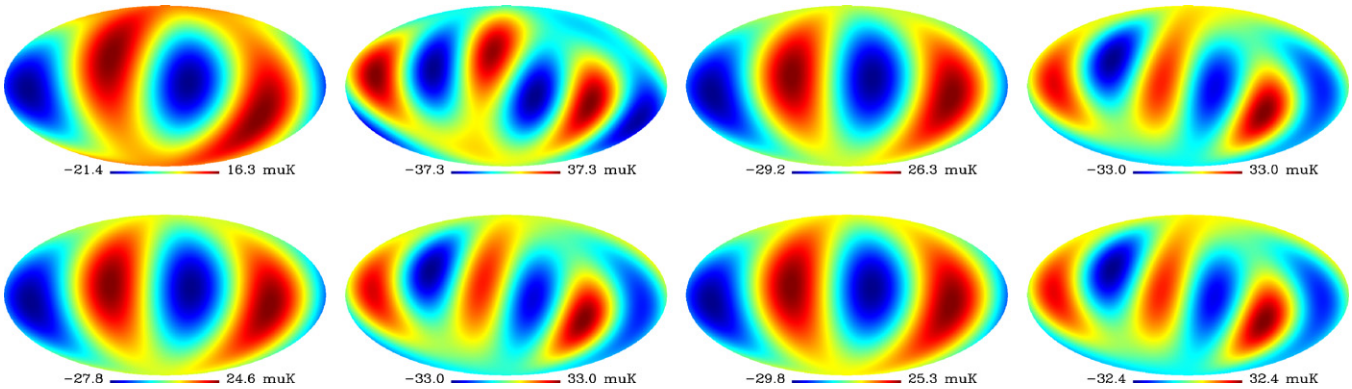

Figure 4. Quadrupole components (left) and octupole components (right) of the ILC map (top) and in-painted maps of the Q, V, and W bands (from the second to the last).

(A color version of this figure is available in the online journal.)

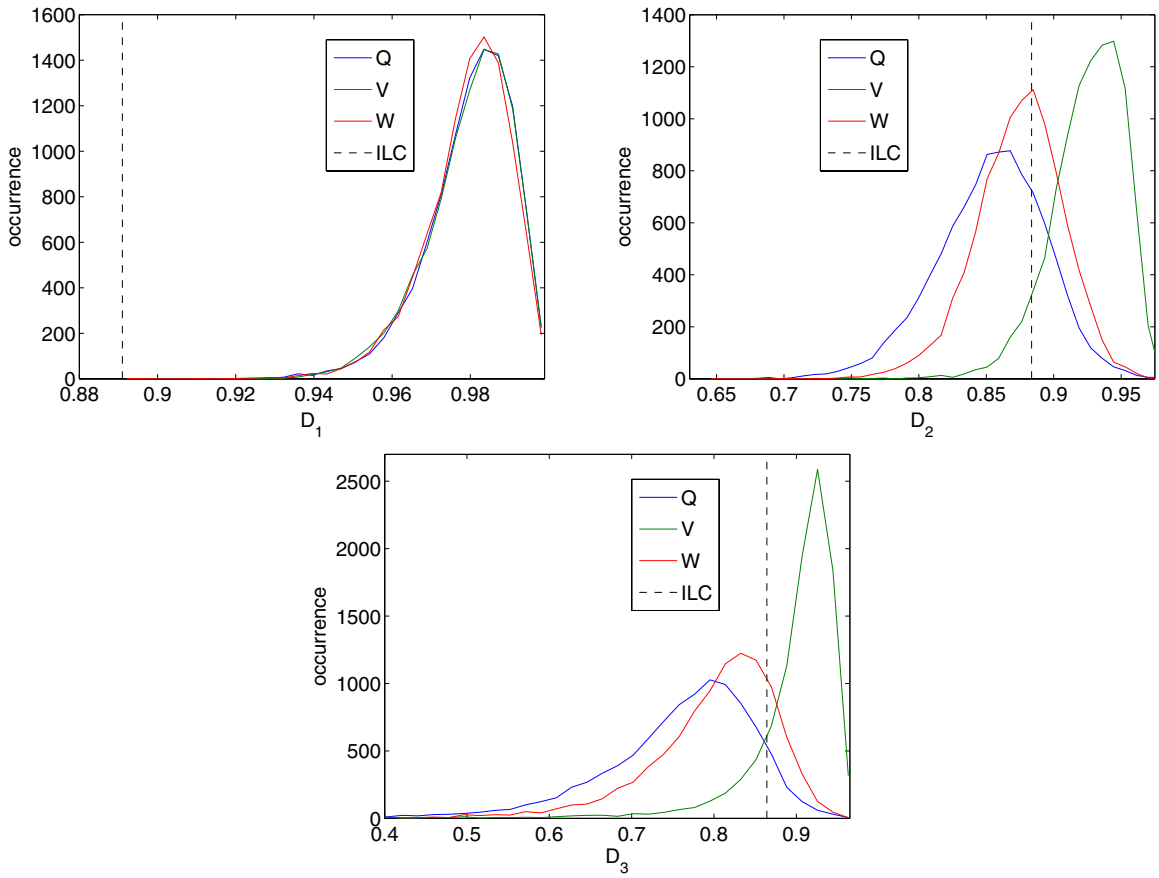

Figure 5. Distribution of the multipole vector alignment between the quadrupole and octupole components of in-painted maps: the alignment of the whole-sky ILC is marked by a dashed line for comparison.

(A color version of this figure is available in the online journal.)

2010a, 2010b; Gruppuso et al. 2011). Further investigation into this issue is deferred to separate publications.

Using the quadrupole and octupole anisotropies of in-painted maps, we investigated the anomalous alignment between the quadrupole and octupole, which are found in the multipole vector analysis of the ILC map (Copi et al. 2004, 2006; Schwarz et al. 2004). In the original study by Copi et al. (2004, 2006) and Schwarz et al. (2004), three dot products D_1, D_2, and D_3 were estimated, where the most anomalous alignment is associated with D_1. Since our in-painting method is statistical, we generated 10,000 in-painted maps for the Q, V, and W, bands, respectively. From each in-painted map, we computed the alignment between multipole vectors, which are quantified by the three dot products D_1, D_2, and D_3, where a higher value of the dot product corresponded to higher alignment (Copi et al. 2004, 2006; Schwarz et al. 2004). In Figure 5, we show the distribution of the dot product values. For D_1, we find that all in-painted maps, except for one in-painted map of the W band, have even higher alignment than the ILC map. It is also interesting to note that the D_2 and D_3 values of the V-band map are much higher than the other bands, even though the V-band map is expected to contain the least foreground contamination. Given our result, we find it difficult to attribute the anomalous alignment to the residual foregrounds.

Previously, Bielewicz et al. (2004, 2005) investigated anisotropy at the lowest multipoles by applying the power equalization filter to the cut-sky foreground-reduced maps. Our result is consistent with their finding that the alignment anomaly is robust with respect to the frequency and sky cut (Bielewicz et al. 2004, 2005).

6. DISCUSSION

Foreground masking leads to large cuts more or less parallel to the Galactic equator and numerous holes in the CMB map. Therefore, there have been a lot of effort put into in-painting of the CMB sky map. Though there have been well-established methods for constrained Monte Carlo simulation for Gaussian fields, the prohibitive computational cost makes it unfeasible for *WMAP* or *Planck* data. In this work, we implemented in-painting in harmonic space, wherein the computational load may be greatly reduced with good approximation. We applied our method to simulated data and the *WMAP* data. It should be kept in mind that the method and the result presented in this work are valid only to the extent that our early universe is Gaussian and statistically isotropic. In the result with the simulated data, we found that the angular correlation of the in-painted maps are in good agreement with the assumed model. Using the in-painted maps of *WMAP* data, we investigated the anomalous alignment between the quadrupole and octupole components, which are originally found in multipole vector analysis of the *WMAP* whole-sky ILC map. From the distribution of D_1 values, we find that the alignment in the foreground-reduced map is even higher than that in the ILC map. It is interesting to note that the *V*-band maps show rather higher alignment than other bands, despite the expectation of the *V*-band map being cleanest. Therefore, we find it hard to attribute the alignment to residual foregrounds. The alignment anomaly, including other anomalies, deserve more rigorous investigations combined with our in-painting method. However, in this Letter, we contend ourselves with demonstrating our method, and defer more rigorous investigation to future publications. For the *Planck* data analysis and future missions, we believe our method will be of great use.

We are grateful to an anonymous referee for thorough reading and comments, which greatly helped us improve the clarity of this work. We acknowledge the use of the Legacy Archive for Microwave Background Data Analysis (LAMBDA). Our data analysis made the use of HEALPix (Gorski et al. 1999; Gorski et al. 2005) and SpICE (Szapudi et al. 2001a, 2001b). This work is supported in part by Danmarks Grundforskningsfond, which allowed the establishment of the Danish Discovery Center.

REFERENCES

Abrial, P., Moudden, Y., Starck, J.-L., et al. 2008, Statist. Methodol., 5, 289
Ballester, C., Bertalmo, M., Caselles, V., Sapiro, G., & Verdera, J. 2001, IEEE Trans. Image Process., 10, 1200
Bertalmo, M., Vese, L., Sapiro, G., & Osher, G. 2003, IEEE Trans. Image Process., 12, 882
Bertschinger, E. 1987, ApJ, 323, L103
Bielewicz, P., Eriksen, H. K., Banday, A. J., Górski, K. M., & Lilje, P. B. 2005, ApJ, 635, 750
Bielewicz, P., Górski, K. M., & Banday, A. J. 2004, MNRAS, 355, 1283
Bucher, M., & Louis, T. 2011, arXiv:1109.0286
Chiang, L.-Y., Naselsky, P. D., Verkhodanov, O. V., & Way, M. J. 2003, ApJ, 590, L65
Coles, P., Dineen, P., Earl, J., & Wright, D. 2004, MNRAS, 350, 989
Copi, C. J., Huterer, D., Schwarz, D. J., & Starkman, G. D. 2006, MNRAS, 367, 79
Copi, C. J., Huterer, D., Schwarz, D. J., & Starkman, G. D. 2010, Adv. Astron., 2010, 847541
Copi, C. J., Huterer, D., Schwarz, D. J., & Starkman, G. D. 2011, arXiv:1103.3505
Copi, C. J., Huterer, D., & Starkman, G. D. 2004, Phys. Rev. D, 70, 043515
de Oliveira-Costa, A., & Tegmark, M. 2006, Phys. Rev. D, 74, 023005
de Oliveira-Costa, A., Tegmark, M., Zaldarriaga, M., & Hamilton, A. 2004, Phys. Rev. D, 69, 063516
Efstathiou, G. 2004, MNRAS, 348, 885
Eriksen, H. K., O'Dwyer, I. J., Jewell, J. B., et al. 2004, ApJ, 155, 227
Feeney, S. M., Peiris, H. V., & Pontzen, A. 2011, Phys. Rev. D, 84, 103002
Gold, B., Odegard, N., Weiland, J. L., et al. 2011, ApJS, 192, 15
Gorski, K. M., Hivon, E., Banday, A. J., et al. 2005, ApJ, 622, 759
Gorski, K. M., Wandelt, B. D., Hansen, F. K., Hivon, E., & Banday, A. J. 1999, (arXiv:astro-ph/9905275)
Gruppuso, A., Finelli, F., Natoli, P., et al. 2011, MNRAS, 411, 1445
Hansen, M., Frejsel, A. M., Kim, J., Naselsky, P., & Nesti, F. 2011, Phys. Rev. D, 83, 103508
Hoffman, Y., & Ribak, E. 1991, ApJ, 380, L5
Hoffman, Y., & Ribak, E. 1992, ApJ, 384, 448
Inoue, K. T., Cabella, P., & Komatsu, E. 2008, Phys. Rev. D, 77, 123539
Jarosik, N., Bennett, C. L., Dunkley, J., et al. 2011, ApJS, 192, 14
Kim, J., & Naselsky, P. 2010a, ApJ, 714, L265
Kim, J., & Naselsky, P. 2010b, Phys. Rev. D, 82, 6
Komatsu, E., Smith, K. M., Dunkley, J., et al. 2011, ApJS, 192, 18
Land, K., & Magueijo, J. 2005a, Phys. Rev. Lett., 95, 071301
Land, K., & Magueijo, J. 2005b, Phys. Rev. D, 72, 101302
Land, K., & Magueijo, J. 2007, MNRAS, 378, 153
Masnou, S. 2002, IEEE Trans. Image Process., 11, 68
Naselsky, P., Hansen, M., & Kim, J. 2011, J. Cosmol. Astropart. Phys., JCAP09(2011)12
Naselsky, P., Zhao, W., Kim, J., & Chen, S. 2012, ApJ, 749, 31
Rakić, A., & Schwarz, D. J. 2007, Phys. Rev. D, 75, 103002
Rane, S. D., Sapiro, G., & Bertalmo, M. 2003, IEEE Trans. Image Process., 12, 296
Schwarz, D. J., Starkman, G. D., Huterer, D., & Copi, C. J. 2004, Phys. Rev. Lett., 93, 221301
Szapudi, I., Prunet, S., & Colombi, S. 2001a, ApJ, 561, L11
Szapudi, I., Prunet, S., Pogosyan, D., Szalay, A. S., & Bond, J. R. 2001b, ApJ, 548, L115
Wandelt, B. D., Larson, D. L., & Lakshminarayanan, A. 2004, Phys. Rev. D, 70, 083511